Resonant light scattering of a laser frequency comb by a quantum dot

K. Konthasinghe, M. Peiris, and A. Muller*
Department of Physics, University of South Florida, Tampa, Florida 33620, USA
(Received 27 May 2014; published 8 August 2014)

We investigate the spectral and temporal properties of light scattered near resonantly by a single quantum dot when the incident laser field is a frequency comb consisting of a superposition of monochromatic waves equidistant in frequency. Such fields encompass those generated by, e.g., a periodically pulsed laser. A general theoretical treatment for the calculation of first- and second-order correlation functions is given which takes account of spectral diffusion through a slowly varying detuning from resonance, permitting accurate comparison with experiments. We explore the two distinct regimes in which the frequency-comb separation is either larger or smaller than the radiative decay rate. We verify the validity of our calculations by a comparison with experimental data for the case of a bichromatic field and discuss the manifestation of phase coherence between the incoming field and the scattered single-photon wave packet.

DOI: 10.1103/PhysRevA.90.023810 PACS number(s): 42.50.Ct, 78.67.Hc, 78.47.−p, 78.55.Cr

I. INTRODUCTION

The near-resonant optical response of a two-level quantum system to an incident laser field, in particular the first- and second-order correlations of the scattered photons, remains an intriguing physical problem, despite its apparent simplicity, from both an experimental and theoretical point of view. Since the seminal work of Mollow describing the spectrum of the light scattered by an atom under strong monochromatic excitation [1], much research has followed, and the topic is now treated in most quantum-optics textbooks. Recently, renewed interest has emerged due to potential applications in quantum-information science [2], in particular using systems other than trapped atoms or ions, such as semiconductor quantum dots (QDs). Of specific relevance is the possibility to interface a large number of quantum systems using resonant light-matter interactions [3–8].

Following the first resonance fluorescence experiments with epitaxial InAs QDs [9–12], significant experimental advances have been reported, most notably the measurement of two-photon indistinguishability [13], correlations in Mollow triplet sidebands [14], coherent light scattering [15–17], light scattering under modulation [18,19], interactions with the semiconductor environment [20], and two-QD light scattering [21]. There has also been significant progress in the theoretical description of resonant light scattering from QDs in the presence of phonons [22,23]. However, the spectral properties of the scattered light have so far primarily been investigated for the case of monochromatic excitation. Although bichromatic resonant light scattering has been studied in atomic beams [24–28] and recently in single QDs [29], to the best of our knowledge, the measurement of the spectrum of the light scattered by a two-state quantum system under strong pulsed excitation has, surprisingly, not been reported before. This is despite theoretical predictions of distinctive features in the resonance fluorescence spectrum, differing from the ordinary Mollow triplet [30–35]. Earlier theoretical work has also focused more specifically on interactions involving a pulse train [36,37].

We investigate here the correlations of the light scattered by a single QD under excitation by a multichromatic field, i.e., a frequency comb, consisting of monochromatic fields evenly spaced in frequency. Although we describe a general formalism, we are interested specifically in the case wherein the multichromatic field corresponds to that of a periodically pulsed laser. We account for slow random spectral fluctuations of the two-level system resonance frequencies, present to some extent in any real system, by a randomly varying detuning. We find a rich structure in the calculated spectra of coherently and incoherently scattered light. Surprisingly, a substantial fraction of the light is scattered coherently, even at large Rabi frequencies. We also calculate the second-order correlation functions in the presence of spectral diffusion and present the results for pulsed excitation under typical experimental conditions. Significantly, the degree of (pulse-integrated) photon antibunching is only high if the temporal width of the pulse is small compared to the radiative lifetime. We verify the validity of our model by a comparison with experimental measurements for the case of bichromatic excitation.

II. THEORETICAL BACKGROUND

We consider a single QD with ground state $|0\rangle$ and excited state $|1\rangle$ (transition frequency ω_0), for which the relevant atomic operators are $S_+ = |1\rangle\langle 0|$, $S_- = |0\rangle\langle 1|$, and $2S_z = |1\rangle\langle 1| - |0\rangle\langle 0|$. Under pulsed laser excitation, the dynamics of the expectation values of these operators are usually obtained by numerically integrating the optical Bloch equations in which the Rabi frequency is taken to be proportional to the temporal envelope of the (single) pulse's electric field. Here we are concerned specifically with a rigorous description of the experimental measurement which results from the time-averaged acquisition of the scattered-light correlations under excitation by millions of single pulses. To capture such time-averaged effects, including coherent light scattering, we describe the incoming pulse train by its constituent monochromatic waves, so that the applied electric field is written as

$$E(t) = \frac{1}{2} e^{-i\omega_s t} \sum_{n=-p}^{p} E_n e^{-i(n\delta t + \phi_n)} + \text{c.c.}, \qquad (1)$$

*mullera@usf.edu

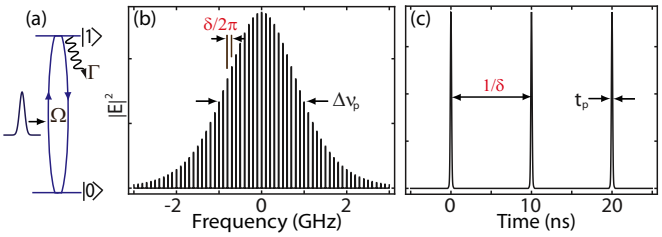

FIG. 1. (Color online) (a) Diagram of a radiatively decaying two-level system driven by a frequency comb. (b) Spectrum of the frequency comb represented by Eq. (1). (c) Temporal profile of a frequency comb with phases ϕ_n and amplitudes E_n such that short pulses of FWHM t_p are obtained.

with time-independent coefficients E_n. The central frequency is ω_s ($n = 0$), and the frequency difference δ (in rad/s) between adjacent waves coincides with 2π times the pulse repetition rate (in Hz). ϕ_n denotes the phase associated with the nth mode of the frequency comb.

Ficek *et al.* have analyzed the fluorescence spectrum of a two-level atom driven by a modulated field in which the central component's frequency coincides with the atom's natural transition frequency, and broadening is determined by spontaneous emission [38]. We extend their treatment to the calculation of the power spectrum and second-order correlation functions with detuning and spectral diffusion, and investigate the scattered-light correlations for the case when the multichromatic field is that of a short pulsed laser excitation (Fig. 1). The optical Bloch equations then read

$$\frac{d\mathbf{X}(t)}{dt} = \mathbf{A}(t)\mathbf{X}(t) + \mathbf{v}, \tag{2}$$

where $\mathbf{X}(t) = (X_1(t), X_2(t), X_3(t))$ with $X_1(t) = \langle \widetilde{S}_-(t)\rangle = \langle S_-(t)\rangle e^{i(\omega_s t+\Psi)}$, $X_2(t) = \langle \widetilde{S}_+(t)\rangle = \langle S_+(t)\rangle e^{-i(\omega_s t+\Psi)}$, $X_3(t) = \langle \widetilde{S}_z(t)\rangle = \langle S_z(t)\rangle$,

$$\mathbf{A}(t) = \begin{pmatrix} -\frac{1}{2}\Gamma - i\Delta & 0 & \sum_{n=-p}^{p} \Omega_n e^{-in\delta t} \\ 0 & -\frac{1}{2}\Gamma + i\Delta & \sum_{n=-p}^{p} \Omega_n^* e^{in\delta t} \\ -\frac{1}{2}\sum_{n=-p}^{p} \Omega_n^* e^{in\delta t} & -\frac{1}{2}\sum_{n=-p}^{p} \Omega_n e^{-in\delta t} & -\Gamma \end{pmatrix}, \tag{3}$$

and $\mathbf{v} = (0,0,-\Gamma/2)$. Here the rotating-wave approximation was made and

$$\Omega_n = \frac{\mu}{\hbar} E_n e^{-i\phi_n}. \tag{4}$$

The radiative decay rate is denoted by Γ, and $\Delta = \omega_0 - \omega_s$ is the detuning from exact resonance. The magnitude of the transition dipole moment, μ, is known to be on the order of 10^{-29} C m for typical InAs QDs [39]. Ψ is an arbitrary phase, chosen here to be $\pi/2$.

In what follows we begin by describing the method for calculating scattered-light spectra under multichromatic excitation (Sec. III), with separate evaluation of coherent (Sec. IV) and incoherent (Sec. V) contributions with and without the effect of spectral diffusion. We proceed with the calculation of second-order correlations in the absence (Sec. VI) and presence (Sec. VII) of spectral diffusion. In Sec. VIII results are then presented for the specific case in which the multichromatic field is produced by a periodically pulsed laser oscillator. Finally, in Sec. IX a side-by-side comparison of our theoretical calculations with experimental data is given for the case of bichromatic excitation.

III. CALCULATION OF THE SCATTERED-LIGHT SPECTRUM

The power spectrum $\mathcal{S}(t,\nu)$ of the light scattered by a two-level quantum system is given by the Fourier transform of the two-time correlation function of the dipole operators [1] as

$$\mathcal{S}(t,\nu) = \Gamma \int_{-\infty}^{\infty} e^{i\nu\tau} \langle S_+(t) S_-(t+\tau)\rangle d\tau. \tag{5}$$

Spectral measurements are typically performed on a time scale much longer than the radiative decay, but also much longer than the phase coherence time (the reciprocal of the linewidth) of the constituent waves of a real frequency comb that Eq. (1) is idealizing. Therefore, the experimental spectrum must be obtained as

$$\mathcal{S}(\nu) = \lim_{T\to\infty} \frac{\delta}{2\pi} \int_{T}^{T+2\pi/\delta} \mathcal{S}(t,\nu) dt, \tag{6}$$

i.e., steady state is assumed and an average over a period $2\pi/\delta$ is performed. With the help of the quantum regression theorem, it can be seen that the two-time correlation functions,

$$\begin{aligned} Y_1(t,\tau) &= \langle \widetilde{S}_+(t)\widetilde{S}_-(t+\tau)\rangle - \langle \widetilde{S}_+(t)\rangle\langle \widetilde{S}_-(t+\tau)\rangle, \\ Y_2(t,\tau) &= \langle \widetilde{S}_+(t)\widetilde{S}_+(t+\tau)\rangle - \langle \widetilde{S}_+(t)\rangle\langle \widetilde{S}_+(t+\tau)\rangle, \\ Y_3(t,\tau) &= \langle \widetilde{S}_+(t)\widetilde{S}_z(t+\tau)\rangle - \langle \widetilde{S}_+(t)\rangle\langle \widetilde{S}_z(t+\tau)\rangle, \end{aligned} \tag{7}$$

satisfy the same equations of motion as $\langle \widetilde{S}_-(t+\tau)\rangle$, $\langle \widetilde{S}_+(t+\tau)\rangle$, and $\langle \widetilde{S}_z(t+\tau)\rangle$, respectively, namely, Eq. (2), with $\mathbf{v} = 0$, $d/dt \to d/d\tau$, and $t \to t+\tau$ [26], i.e.,

$$\frac{d\mathbf{Y}(t,\tau)}{d\tau} = \mathbf{A}(t+\tau)\mathbf{Y}(t,\tau). \tag{8}$$

Thus the power spectrum of the scattered light [Eq. (5)] can be computed if $Y_1(t,\tau)$ is known. Note that $Y_1(t,\tau)$ represents the incoherently scattered radiation since the coherent contribution, $\langle \widetilde{S}_+(t)\rangle\langle \widetilde{S}_-(t+\tau)\rangle$, has been subtracted from the full correlation function $\langle \widetilde{S}_+(t)\widetilde{S}_-(t+\tau)\rangle$. Equation (8) can be solved with the help of the harmonic expansion

$$Y_j(t,\tau) = \sum_{l=-\infty}^{\infty} Y_j^{(l)}(t,\tau) e^{il\delta(t+\tau)} \tag{9}$$

with slowly varying coefficients $Y_j^{(l)}(t,\tau)$, which transforms the problem into an infinite set of equations, written, after a Laplace transform, as

$$z\widehat{Y}_1^{(l)}(z) - Y_1^{(l)}(t,0) = -(\Gamma/2 + i\Delta + il\delta)\widehat{Y}_1^{(l)}(z) + \sum_{n=-p}^{p} \Omega_n \widehat{Y}_3^{(l+n)}(z), \tag{10}$$

$$z\widehat{Y}_2^{(l)}(z) - Y_2^{(l)}(t,0) = -(\Gamma/2 - i\Delta + il\delta)\widehat{Y}_2^{(l)}(z) + \sum_{n=-p}^{p} \Omega_n^* \widehat{Y}_3^{(l-n)}(z), \tag{11}$$

and

$$z\widehat{Y}_3^{(l)}(z) - Y_3^{(l)}(t,0) = -(\Gamma + il\delta)\widehat{Y}_3^{(l)}(z) - \frac{1}{2}\sum_{n=-p}^{p} \left(\Omega_n^* \widehat{Y}_1^{(l-n)}(z) + \Omega_n \widehat{Y}_2^{(l+n)}(z)\right), \tag{12}$$

where $\widehat{Y}_j^{(l)}(z) = \int_0^\infty Y_j^{(l)}(t,\tau)e^{-z\tau}d\tau$.

The set of (complex) coefficients $\{\Omega_n\}_{-p\leqslant n\leqslant p}$, together with the comb spacing δ and the detuning Δ of the central tooth from the natural resonance frequency, specify in full the magnitude and phase of the interaction between the input field and the two-level system. By substitution of Eqs. (10) and (11) into Eq. (12) one then obtains a recursive relation for $\widehat{Y}_3^{(l)}(z)$, written as

$$(z+\Gamma+il\delta)\widehat{Y}_3^{(l)}(z) + \frac{1}{2}\sum_{n,m}\left(\frac{\Omega_n^*\Omega_m}{z+\Gamma/2+i\Delta+i(l-n)\delta}\widehat{Y}_3^{(l-n+m)}(z) + \frac{\Omega_n\Omega_m^*}{z+\Gamma/2-i\Delta+i(l+n)\delta}\widehat{Y}_3^{(l+n-m)}(z)\right) = Y_3^{(l)}(t,0) - \frac{1}{2}\sum_{n}\left(\frac{\Omega_n^* Y_1^{(l-n)}(t,0)}{z+\Gamma/2+i\Delta+i(l-n)\delta} + \frac{\Omega_n Y_2^{(l+n)}(t,0)}{z+\Gamma/2-i\Delta+i(l+n)\delta}\right), \tag{13}$$

where $Y_j^{(l)}(t,0)$ are the initial values of the correlations' expansion coefficients. The initial values of the correlations $Y_j(t,0)$ are given by setting $\tau = 0$ in Eq. (7). Since the calculation of the correlation function in Eq. (6) is at steady state, we can replace $Y_j(t,0)$ with their steady-state values $Y_j^{\rm ss}(t,0)$, which are computed as

$$Y_1^{\rm ss}(t,0) = \tfrac{1}{2} + X_3^{\rm ss}(t) - X_1^{\rm ss}(t)X_2^{\rm ss}(t), \tag{14}$$

$$Y_2^{\rm ss}(t,0) = -X_2^{\rm ss}(t)X_2^{\rm ss}(t), \tag{15}$$

and

$$Y_3^{\rm ss}(t,0) = -\left(\tfrac{1}{2} + X_3^{\rm ss}(t)\right)X_2^{\rm ss}(t), \tag{16}$$

where the superscript "ss" denotes steady state. Using the expansion

$$X_j^{\rm ss}(t) = \sum_{l=-\infty}^{\infty} X_j^{(l)} e^{il\delta t} \tag{17}$$

with time-independent coefficients $X_j^{(l)}$ (steady state) we then obtain

$$Y_1^{(l)}(t,0) = \frac{1}{2}\delta_{l,0} + X_3^{(l)} - \sum_k X_1^{(l-k)}X_2^{(k)}, \tag{18}$$

$$Y_2^{(l)}(t,0) = -\sum_k X_2^{(l-k)}X_2^{(k)}, \tag{19}$$

and

$$Y_3^{(l)}(t,0) = -\sum_k \left(\frac{1}{2}\delta_{k,0} + X_3^{(k)}\right)X_2^{(l-k)}. \tag{20}$$

The coefficients $X_j^{(l)}$ can be found by inserting Eq. (17) into Eq. (2) with $d\mathbf{X}/dt \to 0$ (steady state) which yields the set of equations

$$(\Gamma/2 + i\Delta + il\delta)X_1^{(l)} = \sum_{n=-p}^{p} \Omega_n X_3^{(l+n)}, \tag{21}$$

$$(\Gamma/2 - i\Delta + il\delta)X_2^{(l)} = \sum_{n=-p}^{p} \Omega_n^* X_3^{(l-n)}, \tag{22}$$

and

$$(\Gamma + il\delta)X_3^{(l)} = -\frac{\Gamma}{2}\delta_{l,0} - \frac{1}{2}\sum_{n=-p}^{p}\left(\Omega_n^* X_1^{(l-n)} + \Omega_n X_2^{(l+n)}\right). \tag{23}$$

After substitution of Eqs. (21) and (22) into Eq. (23) one then obtains

$$(\Gamma + il\delta)X_3^{(l)} + \frac{1}{2}\sum_{n,m}\left(\frac{\Omega_n^*\Omega_m}{\Gamma/2+i\Delta+i(l-n)\delta}X_3^{(l-n+m)} + \frac{\Omega_n\Omega_m^*}{\Gamma/2-i\Delta+i(l+n)\delta}X_3^{(l+n-m)}\right) = -\frac{\Gamma}{2}\delta_{0,l}. \tag{24}$$

Once the input field is specified via the set of coefficients $\{\Omega_n\}_{-p\leqslant n\leqslant p}$ in Eq. (4), the calculation of the time-averaged scattered-light spectrum [Eq. (6)] then begins with the computation of $X_3^{(l)}$ using Eq. (24). This can be done, e.g., using the matrix methods described in Ref. [27], in which the harmonic expansions are truncated. With $X_3^{(l)}$ known, $X_1^{(l)}$ and $X_2^{(l)}$ can be computed from Eqs. (21) and (22), respectively. This then allows the calculation of the initial values of the correlations' expansion coefficients using Eqs. (18)–(20), which can be used to solve Eq. (13) for $\widehat{Y}_3^{(l)}(z)$. Finally, $\widehat{Y}_1^{(l)}(z)$ can be computed using Eq. (10).

IV. COHERENTLY-SCATTERED-LIGHT SPECTRUM

A. Radiatively broadened two-level system

The light scattered coherently by a radiatively broadened two-level quantum system has its origins in the equilibrium oscillations of the two-time dipole correlation function. Its spectrum is calculated as the Fourier transform of $\langle S_+(t)\rangle\langle S_-(t+\tau)\rangle$ as

$$\mathcal{S}_{\rm coh}(\nu) = \Gamma \lim_{T\to\infty} \frac{\delta}{2\pi} \times \int_T^{T+2\pi/\delta} \int_{-\infty}^{\infty} e^{i\nu\tau} \langle S_+(t)\rangle\langle S_-(t+\tau)\rangle d\tau dt \tag{25}$$

and therefore by

$$\mathcal{S}_{\rm coh}(\nu) = \Gamma \frac{\delta}{2\pi} \int_0^{2\pi/\delta} \int_{-\infty}^{\infty} e^{i(\nu-\omega_s)\tau} X_2^{\rm ss}(t) X_1^{\rm ss}(t+\tau) d\tau dt \tag{26}$$

or

$$\mathcal{S}_{\rm coh}(\nu) = \Gamma \frac{\delta}{2\pi} \int_0^{2\pi/\delta} \int_{-\infty}^{\infty} e^{i(\nu-\omega_s+l\delta)\tau} \sum_{k,l} X_2^{(k)} X_1^{(l)} e^{i(k+l)\delta t} d\tau dt, \tag{27}$$

and since $X_2^{(-l)} = X_1^{*(l)}$,

$$\mathcal{S}_{\rm coh}(\nu) = 2\pi\Gamma \sum_l \left|X_1^{(l)}\right|^2 \delta_D(\nu-\omega_s+l\delta), \tag{28}$$

where $\delta_D(x)$ denotes the Dirac delta function. The frequency-integrated rate of coherently scattered photons is then given by

$$\gamma_{\rm coh} = \Gamma \sum_l \left|X_1^{(l)}\right|^2, \tag{29}$$

while the total rate of scattered photons is given by

$$\gamma_{\rm tot} = \Gamma\left(\tfrac{1}{2} + X_3^{(0)}\right). \tag{30}$$

B. Radiatively broadened two-level system in the presence of a fluctuating environment

In any real system, particularly in solids, the resonance frequency ω_0 of the two-level system will fluctuate with time. The time scale on which this fluctuation occurs is typically much slower than any other relevant time scales, except for the data acquisition time. Therefore, such effects can be included by simply averaging the spectra obtained for an ideal, radiatively broadened two-level system over a distribution of resonance frequencies.

In the case of InAs QDs, it is well known that random Stark shifts due to fluctuations of the charge density in the surrounding solid matrix are responsible for such spectral diffusion [40]. Although in general the distribution of resulting detunings may be nontrivial [21] it is often sufficient to approximate it with a normal distribution [17]. The resulting spectrum $\overline{\mathcal{S}_{\rm coh}(\nu)}$ is then given by

$$\overline{\mathcal{S}_{\rm coh}(\nu)} = 2\pi\Gamma \sum_l \overline{\left|X_1^{(l)}\right|^2} \delta_D(\nu-\omega_s+l\delta), \tag{31}$$

where

$$\overline{\left|X_1^{(l)}\right|^2} = \frac{1}{\sigma\sqrt{2\pi}} \int_{-\infty}^{\infty} \left|X_1^{(l)}\right|^2 e^{-(\omega_0'-\omega_0)^2/2\sigma^2} d\omega_0'. \tag{32}$$

Here the Gaussian distribution of resonance frequencies has a FWHM, in Hz, of $s/2\pi \approx 2.355\sigma/2\pi$. For InAs QDs epitaxially grown on GaAs, it is typical to measure $s/2\pi \sim 1$ GHz at cryogenic temperatures. Likewise, we obtain the frequency-integrated rate of coherently scattered photons in the presence of spectral diffusion as

$$\overline{\gamma}_{\rm coh} = \Gamma \sum_l \overline{\left|X_1^{(l)}\right|^2}, \tag{33}$$

while the total rate of scattered photons in the presence of spectral diffusion is given by

$$\overline{\gamma}_{\rm tot} = \Gamma\left(\tfrac{1}{2} + \overline{X_3^{(0)}}\right), \tag{34}$$

where

$$\overline{X_3^{(0)}} = \frac{1}{\sigma\sqrt{2\pi}} \int_{-\infty}^{\infty} X_3^{(0)} e^{-(\omega_0'-\omega_0)^2/2\sigma^2} d\omega_0'. \tag{35}$$

V. INCOHERENTLY-SCATTERED-LIGHT SPECTRUM

A. Radiatively broadened two-level system

The spectrum of the light scattered incoherently by an ideal two-level quantum system is given by

$$\mathcal{S}_{\rm inc}(\nu) = \Gamma \lim_{T\to\infty} \frac{\delta}{2\pi} \int_T^{T+2\pi/\delta} \int_{-\infty}^{\infty} Y_1(t,\tau) e^{i(\nu-\omega_s)\tau} d\tau dt, \tag{36}$$

or

$$\mathcal{S}_{\rm inc}(\nu) = 2\Gamma {\rm Re}\left(\widehat{Y}_1^{(0)}(z)\big|_{z=-i(\nu-\omega_s)}\right), \tag{37}$$

where the quantity $\widehat{Y}_1^{(0)}(z)$ is obtained from Eq. (10) with $l=0$.

B. Radiatively broadened two-state system in the presence of a fluctuating environment

When spectral diffusion is present, we obtain the scattered-light spectrum as

$$\overline{\mathcal{S}_{\rm inc}(\nu)} = 2\Gamma {\rm Re}\left(\overline{\widehat{Y}_1^{(0)}(z)}\big|_{z=-i(\nu-\omega_s)}\right), \tag{38}$$

where

$$\overline{\widehat{Y}_1^{(0)}(z)} = \frac{1}{\sigma\sqrt{2\pi}} \int_{-\infty}^{\infty} \widehat{Y}_1^{(0)}(z) e^{-(\omega_0'-\omega_0)^2/2\sigma^2} d\omega_0', \quad (39)$$

with the same parameter σ as for the case of coherently scattered light.

VI. CALCULATION OF SECOND-ORDER CORRELATION FUNCTION

The unnormalized time-averaged second-order correlation function of the scattered light is given by

$$G^{(2)}(\tau) = \frac{\delta}{2\pi} \lim_{T\to\infty} \int_T^{T+2\pi/\delta} \langle S_+(t) S_+(t+\tau) S_-(t+\tau) S_-(t)\rangle dt. \quad (40)$$

With the help of the quantum regression theorem it can be seen that the two-time correlation functions

$$Z_1(t,\tau) = \langle \widetilde{S}_+(t)\widetilde{S}_-(t+\tau)\widetilde{S}_-(t)\rangle - \langle \widetilde{S}_+(t)\widetilde{S}_-(t)\rangle\langle \widetilde{S}_-(t+\tau)\rangle, \quad (41)$$

$$Z_2(t,\tau) = \langle \widetilde{S}_+(t)\widetilde{S}_+(t+\tau)\widetilde{S}_-(t)\rangle - \langle \widetilde{S}_+(t)\widetilde{S}_-(t)\rangle\langle \widetilde{S}_+(t+\tau)\rangle, \quad (42)$$

and

$$Z_3(t,\tau) = \langle \widetilde{S}_+(t)\widetilde{S}_z(t+\tau)\widetilde{S}_-(t)\rangle - \langle \widetilde{S}_+(t)\widetilde{S}_-(t)\rangle\langle \widetilde{S}_z(t+\tau)\rangle, \quad (43)$$

satisfy the same equations of motion as $\langle \widetilde{S}_-(t+\tau)\rangle$, $\langle \widetilde{S}_+(t+\tau)\rangle$, and $\langle \widetilde{S}_z(t+\tau)\rangle$, respectively, namely, Eq. (2), with $\mathbf{v} = 0$, $d/dt \to d/d\tau$, and $t \to t+\tau$, i.e.,

$$\frac{d\mathbf{Z}(t,\tau)}{d\tau} = \mathbf{A}(t+\tau)\mathbf{Z}(t,\tau). \quad (44)$$

Thus $G^{(2)}(\tau)$ can be computed once $Z_3(t,\tau)$ is known. Equation (44) can be solved similarly to Eq. (8) with the help of the harmonic expansion

$$Z_j(t,\tau) = \sum_{l=-\infty}^{\infty} Z_j^{(l)}(t,\tau) e^{il\delta(t+\tau)} \quad (45)$$

with slowly varying coefficients $Z_j^{(l)}(t,\tau)$. Note that in the final evaluation process the sum in Eq. (45) will be truncated to some large integer so that an arbitrary degree of precision can be achieved. This expansion transforms the problem into one involving an infinite set of equations written, after a Laplace transform, as

$$z\widehat{Z}_1^{(l)}(z) - Z_1^{(l)}(t,0) = -(\Gamma/2 + i\Delta + il\delta)\widehat{Z}_1^{(l)}(z) + \sum_{n=-p}^{p} \Omega_n \widehat{Z}_3^{(l+n)}(z), \quad (46)$$

$$z\widehat{Z}_2^{(l)}(z) - Z_2^{(l)}(t,0) = -(\Gamma/2 - i\Delta + il\delta)\widehat{Z}_2^{(l)}(z) + \sum_{n=-p}^{p} \Omega_n^* \widehat{Z}_3^{(l-n)}(z), \quad (47)$$

and

$$z\widehat{Z}_3^{(l)}(z) - Z_3^{(l)}(t,0) = -(\Gamma + il\delta)\widehat{Z}_3^{(l)}(z) - \frac{1}{2}\sum_{n=-p}^{p} \left(\Omega_n^* \widehat{Z}_1^{(l-n)}(z) + \Omega_n \widehat{Z}_2^{(l+n)}(z)\right). \quad (48)$$

After solving for $\widehat{Z}_1^{(l)}(z)$ in Eq. (46) and for $\widehat{Z}_2^{(l)}(z)$ in Eq. (47) and substituting the results into Eq. (48), one obtains a recursive relation for $\widehat{Z}_3^{(l)}(z)$, written as

$$(z+\Gamma+il\delta)\widehat{Z}_3^{(l)}(z) + \frac{1}{2}\sum_{n,m}\left(\frac{\Omega_n^*\Omega_m}{z+\Gamma/2+i\Delta+i(l-n)\delta}\widehat{Z}_3^{(l-n+m)}(z) + \frac{\Omega_n\Omega_m^*}{z+\Gamma/2-i\Delta+i(l+n)\delta}\widehat{Z}_3^{(l+n-m)}(z)\right) = Z_3^{(l)}(t,0) - \frac{1}{2}\sum_{n}\left(\frac{\Omega_n^* Z_1^{(l-n)}(t,0)}{z+\Gamma/2+i\Delta+i(l-n)\delta} + \frac{\Omega_n Z_2^{(l+n)}(t,0)}{z+\Gamma/2-i\Delta+i(l+n)\delta}\right), \quad (49)$$

where $Z_j^{(l)}(t,0)$ are the initial values of the correlations' expansion coefficients. The initial values of the correlations $Z_j(t,0)$ are given by setting $\tau = 0$ in Eqs. (41)–(43). Since the calculation of $G^{(2)}(\tau)$ is at steady state, we can replace $Z_j(t,0)$ with their steady-state values $Z_j^{ss}(t,0)$, which are computed as

$$Z_1^{ss}(t,0) = -\left(X_3^{ss}(t) + 1/2\right)X_1^{ss}(t), \quad (50)$$

$$Z_2^{ss}(t,0) = -\left(X_3^{ss}(t) + 1/2\right)X_2^{ss}(t), \quad (51)$$

$$Z_3^{ss}(t,0) = -\left(X_3^{ss}(t) + 1/2\right)^2. \quad (52)$$

Using again the expansion in Eq. (17), with time-independent coefficients $X_j^{(l)}$ (steady state) we then obtain

$$Z_1^{(l)}(t,0) = -\frac{1}{2}X_1^{(l)} - \sum_k X_1^{(k)} X_3^{(l-k)}, \quad (53)$$

$$Z_2^{(l)}(t,0) = -\frac{1}{2}X_2^{(l)} - \sum_k X_2^{(k)} X_3^{(l-k)}, \quad (54)$$

$$Z_3^{(l)}(t,0) = -\frac{1}{4}\delta_{l,0} - X_3^{(l)} - \sum_k X_3^{(k)} X_3^{(l-k)}. \quad (55)$$

With the initial values known, the second-order correlation function ($\tau > 0$) is then given as

$$G^{(2)}(\tau) = \mathcal{F}^{-1}\left\{2\mathrm{Re}\widehat{Z}_3^{(0)}(z)\big|_{z=-i\nu'}\right\} + \sum_k X_3^{(k)} X_3^{(-k)} e^{ik\delta\tau} + X_3^{(0)} + \frac{1}{4}, \quad (56)$$

where $\mathcal{F}^{-1}$ denotes the inverse Fourier transform with respect to ν', defined as

$$\mathcal{F}^{-1}\{f(\nu')\} = \frac{1}{2\pi}\int_{-\infty}^{\infty} f(\nu') e^{-i\nu'\tau} d\nu'. \quad (57)$$

The quantity usually measured in an experiment is proportional to the normalized second-order correlation function of the scattered light defined as

$$g^{(2)}(\tau) = G^{(2)}(\tau)/N, \quad (58)$$

where N is a normalization factor given by

$$N = \frac{\delta}{2\pi}\lim_{T\to\infty}\int_T^{T+2\pi/\delta} \langle S_+(t)S_-(t)\rangle^2 dt. \quad (59)$$

This normalization factor can be computed as

$$N = \frac{1}{4} + X_3^{(0)} + \sum_k X_3^{(k)} X_3^{(-k)}. \quad (60)$$

Thus for obtaining the desired normalized second-order correlation function [Eq. (58)], Eq. (49) must first be solved for $\widehat{Z}_3^{(l)}(z)$. For this calculation the initial values of the second-order correlation expansion function coefficients must be first obtained using Eqs. (53)–(55) using the X_j obtained before with Eqs. (21), (22), and (24).

VII. SECOND-ORDER CORRELATION FUNCTION IN THE PRESENCE OF A FLUCTUATING ENVIRONMENT

In the presence of a slowly varying, normally distributed, random detuning, as in Secs. IV B and V B, we must further perform an average of the second-order correlation functions over these detunings as

$$g_{\mathrm{av}}^{(2)}(\tau) = \overline{G^{(2)}(\tau)}/\overline{N}, \quad (61)$$

where

$$\overline{G^{(2)}(\tau)} = \frac{1}{\sigma\sqrt{2\pi}}\int_{-\infty}^{\infty} G^{(2)}(\tau) e^{-(\omega_0'-\omega_0)^2/2\sigma^2} d\omega_0' \quad (62)$$

and

$$\overline{N} = \frac{1}{\sigma\sqrt{2\pi}}\int_{-\infty}^{\infty} N e^{-(\omega_0'-\omega_0)^2/2\sigma^2} d\omega_0'. \quad (63)$$

VIII. SCATTERED-LIGHT CORRELATIONS UNDER MODE-LOCKED LASER FREQUENCY-COMB EXCITATION

We now numerically evaluate the first- and second-order correlations of light scattered by a QD for the specific case for which the incoming field's temporal envelope is given by the function

$$\mathcal{E}(t) = \sum_{n=0}^{\infty} \mathcal{E}_s\left(t - \frac{2\pi n}{\delta}\right), \quad (64)$$

with

$$\mathcal{E}_s(t) = \mathcal{E}_0 \mathrm{sech}(1.76t/t_p), \quad (65)$$

where t_p is the FWHM of the temporal *intensity* profile of a single pulse. Mode-locked laser oscillators commonly produce such pulse trains, for which the time-bandwidth product is $t_p\Delta\nu_p \approx 0.315$, where $\Delta\nu_p$ is the FWHM, in Hz, of the pulse's power spectrum. We will further assume that the laser cavity has been sufficiently stabilized so that over the measurement duration we can describe the applied field by

$$E(t) = \mathcal{E}(t)\cos(\omega_s t), \quad (66)$$

and thus in the notation of Eq. (1), $\phi_n = 0$ and

$$E_n = \frac{\delta}{2\pi}\int_{-\pi/\delta}^{\pi/\delta} \mathcal{E}_s(t) e^{in\delta t} dt. \quad (67)$$

The laser's power spectrum is then given by

$$\mathcal{S}_{\mathrm{laser}}(\nu) \propto 2\pi \sum_{n=-p}^{p} |E_n|^2 \delta_D(\nu - \omega_s - n\delta). \quad (68)$$

Note that the detection frequency ν is denoted in circular measure. Thus, together with the detuning Δ, the pulse width t_p and the (temporal) peak Rabi frequency $\Omega_R = |\mu\mathcal{E}_0|/\hbar$ quantify the strength of the interaction between the QD and the laser pulse. Since we are concerned here with the time-averaged interaction involving a large number of pulses, the magnitude of the pulse repetition period, $2\pi/\delta$, relative to the QD radiative lifetime, $2\pi/\Gamma$, is another determinant factor for the magnitude of the average interaction strength. In particular we must distinguish whether prior to the arrival of a subsequent pulse the QD has returned to its ground state ($\delta < \Gamma$) or not. We define the input pulse area θ in the usual way as

$$\theta = \frac{\mu}{\hbar}\int_{-\infty}^{\infty} \mathcal{E}_s(t) dt = \Omega_R \frac{\pi t_p}{1.76} \quad (69)$$

to describe maxima ($\theta = \pi, 3\pi, 5\pi$, etc.) or minima ($\theta = 2\pi, 4\pi, 6\pi$, etc.) of the population of the two-level system after passage of the pulse. Throughout we will assume that the radiative decay rate of the QD is $\Gamma/2\pi = 200$ MHz, consistent with the radiative lifetime of $\sim$1 ns typically measured for InAs QDs [41].

A. Regime in which the radiative lifetime is shorter than the pulse repetition period ($\delta < \Gamma$)

We begin with the specific case in which the pulse repetition rate is fixed at $\delta/2\pi = 100$ MHz (as in, e.g., a table-top Ti:sapphire oscillator), and the temporal pulse width is $t_p = 800$ ps ($\Delta\nu_p \approx 0.39$ GHz). The corresponding field intensity as a function of time is represented in Fig. 2(a). Making use of Eqs. (29), (30), (33), and (34), we represent the rate of photons scattered coherently, incoherently, and their sum, with and without including the effect of spectral diffusion, as a function of pulse area θ [Fig. 2(b)]. It can be seen that for $\theta < \pi$ the scattered-light intensity is dominated by coherent

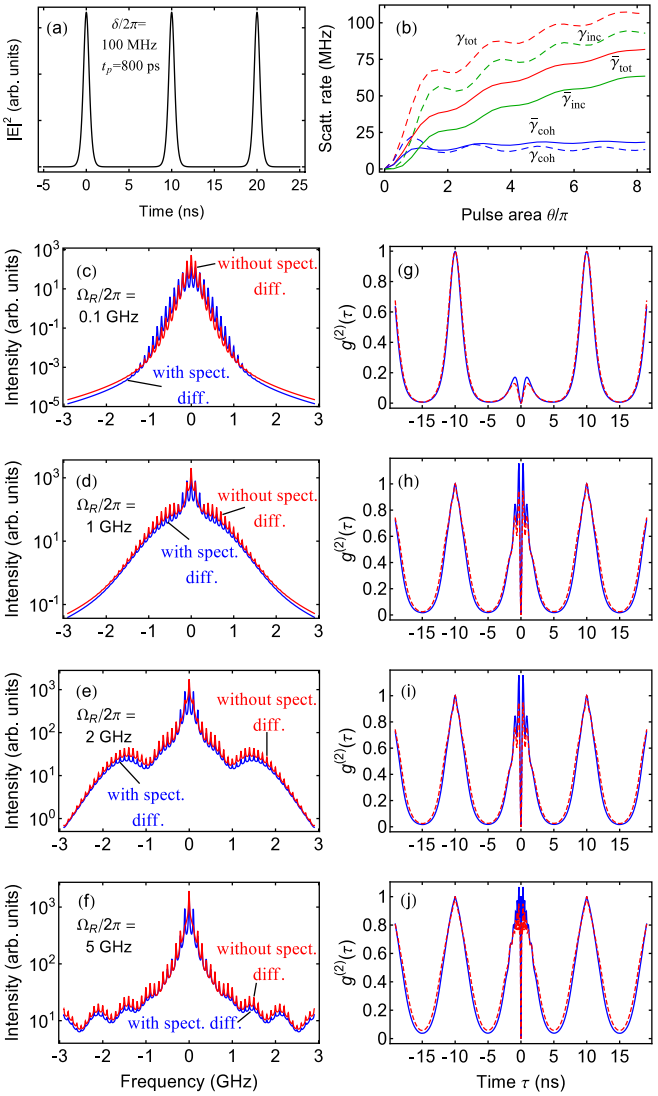

FIG. 2. (Color online) (a) Temporal envelope of the applied field's intensity. (b) Intensity of total ($\gamma_{\rm tot}$, $\overline{\gamma}_{\rm tot}$, red), coherently ($\gamma_{\rm coh}$, $\overline{\gamma}_{\rm coh}$, blue), and incoherently ($\gamma_{\rm inc} = \gamma_{\rm tot} - \gamma_{\rm coh}$, $\overline{\gamma}_{\rm inc} = \overline{\gamma}_{\rm tot} - \overline{\gamma}_{\rm coh}$, green) scattered light, calculated with (solid lines) and without (dashed lines) spectral diffusion. (c)–(f) Calculated spectra of scattered light for the applied field in Fig. 2(a) with Rabi frequencies $\Omega_R/2\pi = 0.1$, 1, 2, and 5 GHz, respectively, with (blue) and without (red) spectral diffusion. These correspond to pulse areas of $\theta = 0.3\pi$, 3.0π, 5.7π and 14.3π, respectively. (g)–(j) Calculated second-order correlation functions under the same conditions with (solid blue line) and without (dashed red line) spectral diffusion.

scattering, as anticipated, whereas for $\theta > \pi$, incoherent scattering dominates. However, unlike the monochromatic case in which the intensity of coherently scattered photons keeps decreasing with Rabi frequency, it remains steady for the pulsed case. Furthermore, it is also seen from Fig. 2(b) that the effect of spectral diffusion is generally to increase the fraction of coherently scattered photons for a given Rabi frequency.

In Figs. 2(c)–2(j) the power spectrum (left) and second-order correlation function (right) are plotted with (blue) and without (red) inclusion of spectral diffusion for increasing Rabi frequency Ω_R from top to bottom. It is seen that the

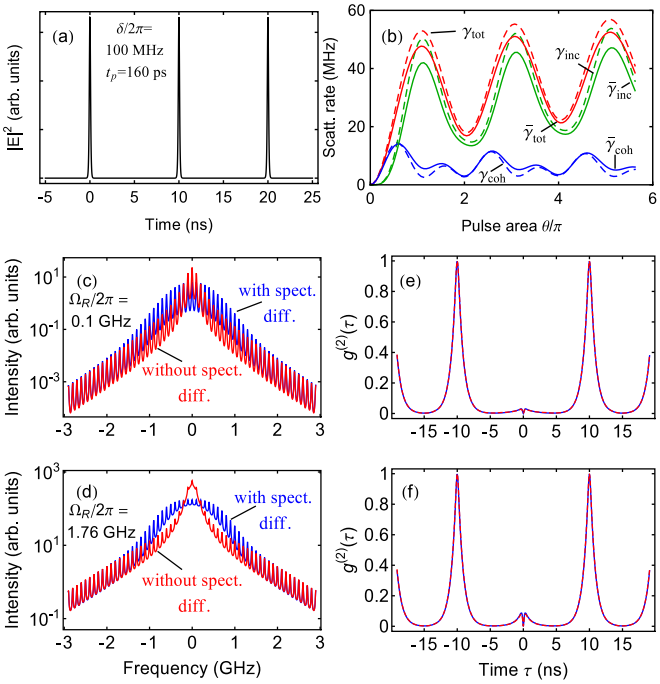

FIG. 3. (Color online) (a) Temporal envelope of the applied field's intensity. (b) Intensity of total ($\gamma_{\rm tot}$, $\overline{\gamma}_{\rm tot}$, red), coherently ($\gamma_{\rm coh}$, $\overline{\gamma}_{\rm coh}$, blue) and incoherently ($\gamma_{\rm inc} = \gamma_{\rm tot} - \gamma_{\rm coh}$, $\overline{\gamma}_{\rm inc} = \overline{\gamma}_{\rm tot} - \overline{\gamma}_{\rm coh}$, green) scattered light, calculated with (solid lines) and without (dashed lines) spectral diffusion. (c)–(d) Calculated spectra of scattered light for the applied field in Fig. 3(a) with pulse areas $\theta = 0.06\pi$ ($\Omega_R/2\pi = 0.1$ GHz) and $\theta = \pi$ ($\Omega_R/2\pi = 1.76$ GHz), respectively, with (blue) and without (red) spectral diffusion. (e)–(f) Calculated second-order correlation function under the same conditions with (solid blue line) and without (dashed red line) spectral diffusion.

dominant sidebands are separated from the central frequency by approximately $\pm\Omega_R/2\pi$, as in the conventional Mollow triplet [1]. In addition, other sidebands are present which are closer to the central peak than the dominant sidebands. These are most visible at the largest Rabi frequencies. The light scattered coherently appears in the form of a comb, for which a 20 MHz convolution has been applied to mimic a realistic instrument response function.

It is interesting to see that even for a small pulse area [Fig. 2(g)], pulse-integrated photon antibunching is incomplete, in the sense that the area around the central peak ($\tau = 0$) does not vanish. This changes when we decrease the temporal duration of the pulse. Figure 3 shows the case where the temporal pulse width is now reduced to $t_p = 160$ ps. The corresponding spectral width of the frequency comb is then $\Delta\nu_p \approx 2$ GHz. Although pulse-integrated photon antibunching is suppressed for large Rabi frequencies, it is now clearly taking place for $\theta \ll \pi$ [Fig. 3(e)]. With increasing spectral bandwidth of the frequency comb, the effect of spectral diffusion is also more visible, but only in the scattered-light spectrum [Figs. 3(c) and 3(d)]. The second-order correlation functions are not affected significantly by spectral diffusion [Figs. 3(e) and 3(f)].

As we further decrease the temporal pulse width, these trends continue. In Fig. 4, the pulse width is now 50 ps ($\Delta\nu_p \approx 6.3$ GHz). The scattered light spectra and correlations

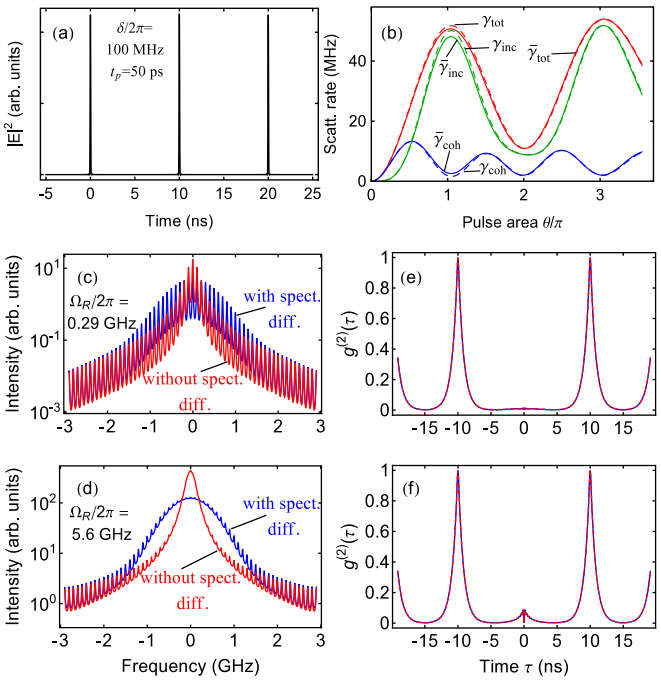

FIG. 4. (Color online) (a) Temporal envelope of the applied field's intensity. (b) Intensity of total ($\gamma_{\rm tot}$, $\overline{\gamma}_{\rm tot}$, red), coherently ($\gamma_{\rm coh}$, $\overline{\gamma}_{\rm coh}$, blue), and incoherently ($\gamma_{\rm inc}=\gamma_{\rm tot}-\gamma_{\rm coh}$, $\overline{\gamma}_{\rm inc}=\overline{\gamma}_{\rm tot}-\overline{\gamma}_{\rm coh}$, green) scattered light, calculated with (solid lines) and without (dashed lines) spectral diffusion. (c)–(d) Calculated spectra of scattered light for the applied field in Fig. 4(a) with pulse areas $\theta=0.05\pi$ ($\Omega_R/2\pi=0.29$ GHz) and $\theta=\pi$ ($\Omega_R/2\pi=5.6$ GHz), respectively, with (blue) and without (red) spectral diffusion. (e)–(f) Calculated second-order correlation function under the same conditions with (solid blue line) and without (dashed red line) spectral diffusion.

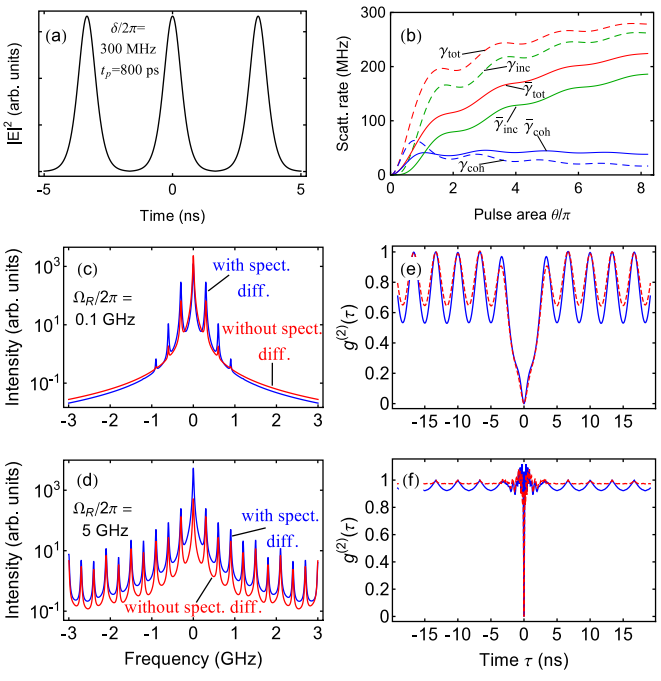

FIG. 5. (Color online) (a) Temporal envelope of the applied field's intensity. (b) Intensity of total ($\gamma_{\rm tot}$, $\overline{\gamma}_{\rm tot}$, red), coherently ($\gamma_{\rm coh}$, $\overline{\gamma}_{\rm coh}$, blue) and incoherently ($\gamma_{\rm inc}=\gamma_{\rm tot}-\gamma_{\rm coh}$, $\overline{\gamma}_{\rm inc}=\overline{\gamma}_{\rm tot}-\overline{\gamma}_{\rm coh}$, green) scattered light, calculated with (solid lines) and without (dashed lines) spectral diffusion. (c)–(d) Calculated spectra of scattered light for the applied field in Fig. 5(a) with pulse areas $\theta=0.29\pi$ ($\Omega_R/2\pi=0.1$ GHz) and $\theta=22\pi$ ($\Omega_R/2\pi=5$ GHz), respectively, with (blue) and without (red) spectral diffusion. (e)–(f) Calculated second-order correlation function under the same conditions with (solid blue line) and without (dashed red line) spectral diffusion.

are shown for $\theta=0.05\pi$ and $\theta=\pi$, which corresponds to $\Omega_R/2\pi=0.29$ GHz and $\Omega_R/2\pi=5.6$ GHz, respectively. The effect of spectral diffusion is striking, but only for the spectral correlations [Figs. 4(c) and 4(d)], and the probability of emitting two photons in the same pulse is very small only when $\theta\ll\pi$ [Fig. 4(e)].

With decreasing temporal pulse width the spectral width of the excitation source will eventually exceed significantly the natural linewidth Γ of the transition. It is then expected that spectral components at the edge of the spectrum will not contribute to the correlations of the scattered light due to their off-resonance character. In fact, the determinant factor is whether the detuning of these spectral components is larger than either the spectral diffusion broadened linewidth s or the Rabi frequency Ω_R, whichever is greater, i.e., modes for which

$$n\gtrsim\frac{\max(s,\Omega_R)}{\delta} \tag{70}$$

can be safely ignored. Thus, truncation of the excitation field's spectral decomposition [Eq. (1)] can be made at $p\approx\max(s,\Omega_R)/\delta$ when carrying out the numerical evaluations.

B. Regime in which the radiative lifetime is longer than the pulse repetition period ($\delta>\Gamma$)

When the pulse repetition period is shorter than the radiative lifetime, then the two-level system population does not have time to return to the ground state before the arrival of a subsequent pulse. This situation corresponds to a comb teeth separation exceeding the QD linewidth. In Fig. 5 we show the spectra calculated for such a case when $\delta/2\pi=300$ MHz, and $t_p=800$ ps for weak and strong excitation. Subsequent peaks in the second-order correlation functions now significantly overlap and the latter are more sensitive to spectral diffusion.

When reducing the temporal pulse width down to 160 ps (Fig. 6), the correlations overall resemble still closely those observed for lower pulse repetition rates (Fig. 3). In particular, Rabi oscillations are clearly seen [Fig. 6(b)], and dominant spectral sidebands are visible [Fig. 6(d)] at a separation from the central frequency of approximately $\pm\Omega_R/2\pi$.

Finally, when the pulse repetition rate is exceedingly large (Fig. 7) the interaction involves in effect only several modes of the comb. Although pulse-area-dependent Rabi oscillations still remain visible [Fig. 7(b)], the photon correlations resemble more closely those observed under monochromatic excitation. Both spectral and temporal correlations are affected significantly by spectral diffusion.

IX. BICHROMATIC EXCITATION

To confirm the validity of our calculations, we compare the correlations evaluated numerically using the formalism

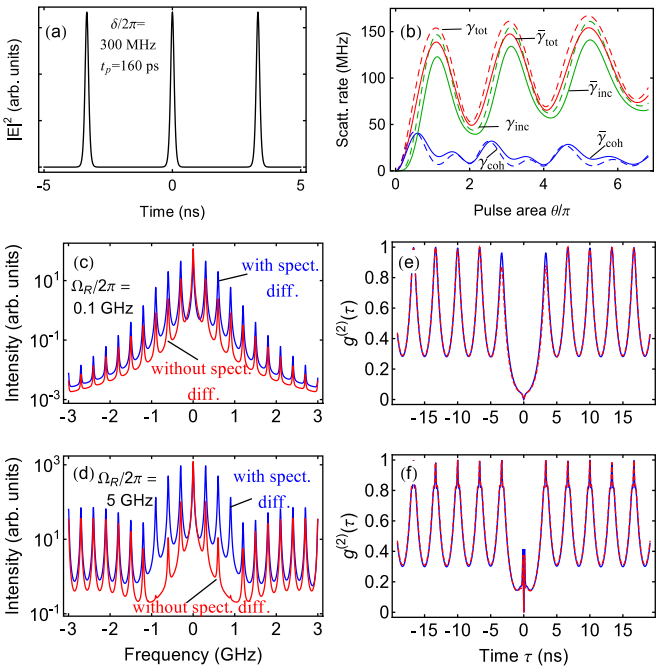

FIG. 6. (Color online) (a) Temporal envelope of the applied field's intensity. (b) Intensity of total (γ_{tot}, $\overline{\gamma}_{tot}$, red), coherently (γ_{coh}, $\overline{\gamma}_{coh}$, blue) and incoherently ($\gamma_{inc} = \gamma_{tot} - \gamma_{coh}$, $\overline{\gamma}_{inc} = \overline{\gamma}_{tot} - \overline{\gamma}_{coh}$, green) scattered light, calculated with (solid lines) and without (dashed lines) spectral diffusion. (c)–(d) Calculated spectra of scattered light for the applied field in Fig. 6(a) with pulse areas $\theta = 0.06\pi$ ($\Omega_R/2\pi = 0.1$ GHz) and $\theta = 2.9\pi$ ($\Omega_R/2\pi = 5$ GHz), respectively, with (blue) and without (red) spectral diffusion. (e)–(f) Calculated second-order correlation function under the same conditions with (solid blue line) and without (dashed red line) spectral diffusion.

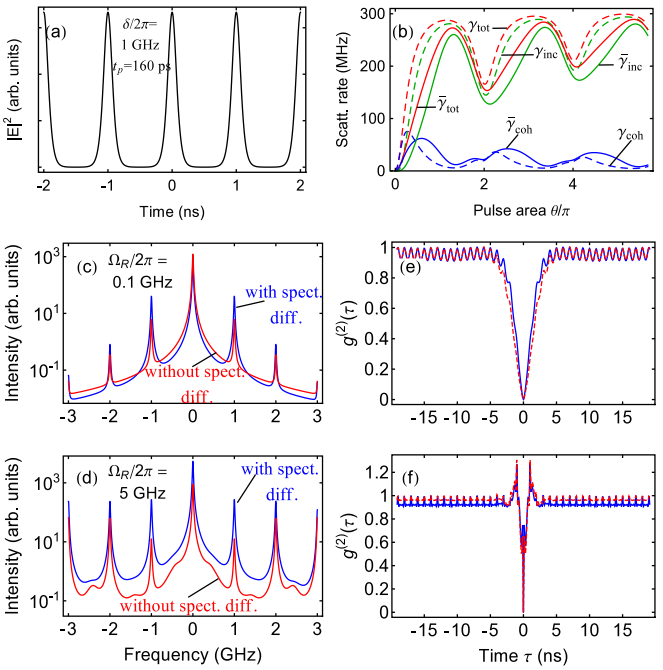

FIG. 7. (Color online) (a) Temporal envelope of the applied field's intensity. (b) Intensity of total (γ_{tot}, $\overline{\gamma}_{tot}$, red), coherently (γ_{coh}, $\overline{\gamma}_{coh}$, blue) and incoherently ($\gamma_{inc} = \gamma_{tot} - \gamma_{coh}$, $\overline{\gamma}_{inc} = \overline{\gamma}_{tot} - \overline{\gamma}_{coh}$, green) scattered light, calculated with (solid lines) and without (dashed lines) spectral diffusion. (c)–(d) Calculated spectra of scattered light for the applied field in Fig. 7(a) with pulse areas $\theta = 0.06\pi$ ($\Omega_R/2\pi = 0.1$ GHz) and $\theta = 2.9\pi$ ($\Omega_R/2\pi = 5$ GHz), respectively, with (blue) and without (red) spectral diffusion. (e)–(f) Calculated second-order correlation function under the same conditions with (solid blue line) and without (dashed red line) spectral diffusion.

described above with experimental data recorded for the case of bichromatic excitation [29]. Bichromatic excitation corresponds to $p = 1$ and thus a set of three coefficients $(\Omega_{-1}, 0, \Omega_1)$ characterize the strength of the interaction [Eq. (4)]. The first laser, associated with the Rabi frequency $\Omega_{-1}/2\pi$, is detuned from the second laser, associated with the Rabi frequency $\Omega_1/2\pi$, by $2\delta/2\pi$. Furthermore, the average frequency of the two lasers is detuned by an amount $\Delta/2\pi$ from the QD resonance frequency. A least-squares fitting was performed to include the effect of spectral diffusion, for which the free parameters were a scale factor and the FWHM of the distribution of resonance frequencies due to spectral diffusion, $s/2\pi$, defined in Eq. (32). The best-fit values for the latter were found to be close to the value obtained by extrapolating the FWHM of the single laser excitation spectrum to the limit of vanishing Rabi frequency, i.e. $s/2\pi \approx 1$ GHz. For both cases presented in Fig. 8, the two lasers used had the same intensity, such that $\Omega_{-1}/2\pi = \Omega_1/2\pi = 1$ GHz, and $\Omega_0 = 0$. However, the frequency difference between the two lasers was $2\delta/2\pi = 0.86$ GHz in the experiment of Fig. 8(a) and $2\delta/2\pi = 1.56$ GHz in the experiment of Fig. 8(b). Thus the effective interaction between the external field and the QD is stronger in Fig. 8(a) than it is in Fig. 8(b). Accordingly, more peaks are observed in the former case. These peaks can be regarded as arising from transitions between subsequent manifolds of the "dressed states ladder" which is composed of an infinite number of levels for $p \geqslant 1$ [29]. Differences are visible when spectral diffusion is included. In particular, the magnitude of the sharp peaks corresponding to coherent light scattering are faithfully represented only when spectral diffusion is included.

Second-order correlations measured for the case of bichromatic light scattering were also compared to our theoretical calculations (Fig. 9). As for excitation with broader frequency combs discussed above, spectral diffusion has a lesser effect on the second-order correlations than it has on the scattered-light spectra. Nonetheless, subtle differences can be seen in Fig. 9 when computing the theoretical functions with (blue traces) and without (red, dashed traces) spectral diffusion. The persisting oscillations visible at long correlation time occur at the frequency $2\delta/2\pi$.

We finally note that we have also compared the results of our calculations using the formalism presented here with a direct numerical integration of differential equations obeyed by the relevant correlation functions. Such an approach leads to similar results, but can be computationally intensive, in particular for the calculation of scattered-light spectra involving dense frequency combs. It also lacks some of the insights provided by the spectral decomposition used here, such as the separation of coherent and incoherent scattering.

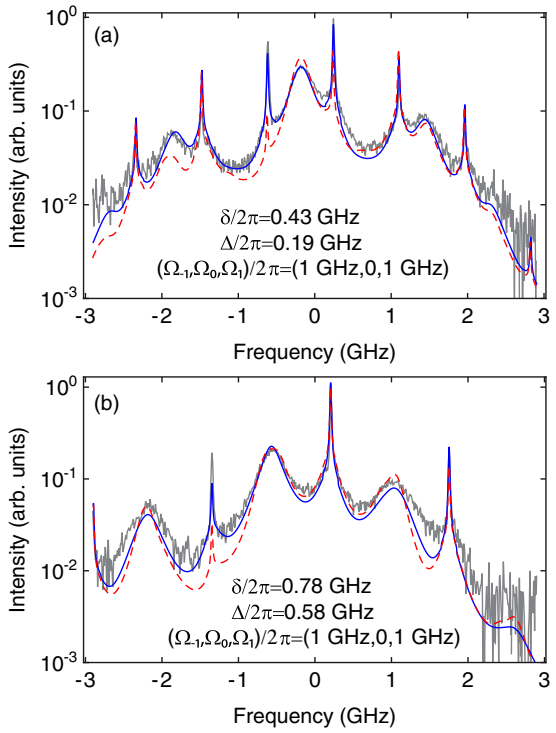

FIG. 8. (Color online) (a) Experimental (gray solid line) and theoretical scattered-light spectra under bichromatic excitation with parameters $\delta, \Delta, \Omega_{-1}$, and Ω_1 as indicated. The theoretical spectrum is computed with (blue) and without (red, dashed) spectral diffusion. (b) Scattered-light spectra as in (a) but with different δ and Δ as indicated.

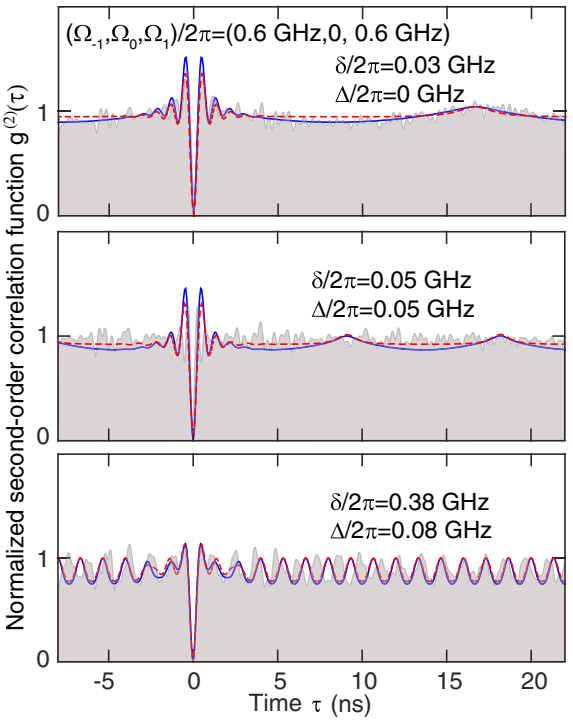

FIG. 9. (Color online) Experimental (gray solid shaded area) and theoretical scattered-light second-order correlation functions under bichromatic excitation for δ and Δ as indicated, with (blue) and without (red, dashed) spectral diffusion.

X. DISCUSSION

A. Scattered wave-packet properties

A number of potential applications in quantum-information science rely upon processes involving single or few photons, and often specific spectral and temporal characteristics are needed. It is therefore of interest to determine the "shape" of the photon wave packets generated in the resonant light-scattering process investigated here.

The properties of the scattered wave packets can be inferred from the mean value of the scattered electric field. The positive frequency part of the latter at position $\mathbf{r}$ can be related to the atomic lowering operator by [1]

$$\left\langle \mathbf{E}^{(+)}_{\rm scatt}(\mathbf{r},t)\right\rangle = \mathbf{f}(\mathbf{r})\langle S_-(t-r/c)\rangle, \tag{71}$$

where $\mathbf{f}(\mathbf{r})$ denotes the spatial distribution of the radiation generated during the scattering process. In the case of a dipole in bulk, the spatial function $\mathbf{f}(\mathbf{r})$ is given by

$$\mathbf{f}(\mathbf{r}) = \frac{\omega_0^2\mu}{4\pi\epsilon_0 c^2 r}(\hat{\mathbf{r}}\times\hat{\mathbf{e}}_\mu)\times\hat{\mathbf{r}}, \tag{72}$$

where $\hat{\mathbf{e}}_\mu$ is a unit vector along the dipole. In the presence of nearby reflecting surfaces, as is commonly the case in experiments with QDs, $\mathbf{f}(\mathbf{r})$ is modified compared to the bulk case. In particular, using a microresonator, the spatial pattern can be tailored so that the scattered light is directed in a preferred direction. We assume here that the QD is placed inside a microresonator such that most of the scattered photons can be collected, e.g., into an optical fiber, without significantly modifying the total rate of scattering compared to the bulk case. The electric field associated with these photons is then given, at steady state, by

$$\langle E_{\rm scatt}(\mathbf{r},t+r/c)\rangle = \frac{|\mathbf{f}(\mathbf{r})|}{2}e^{-i(\omega_s t+\Psi_s)}\sum_{l=-k}^{k}X_1^{(l)}e^{il\delta t} + \frac{|\mathbf{f}(\mathbf{r})|}{2}e^{+i(\omega_s t+\Psi_s)}\sum_{l=-k}^{k}X_2^{(l)}e^{il\delta t}. \tag{73}$$

According to Eq. (73) the scattered electric field is directly associated with the coefficients $X_1^{(l)}$, the magnitude of which is in turn proportional to the rate of coherently scattered light [Eq. (29)]. Since the fraction of coherently scattered light remains elevated, even at large Rabi frequencies, a portion of the scattered light always maintains a fixed phase relationship with the incoming laser. An interesting situation thus arises when the input pulse area is less than π, since in that regime a high degree of pulse-integrated photon antibunching also indicates that only a single photon can be scattered at most for one laser pulse. The temporal "shape" of the corresponding wave packet is then that of a decaying exponential (with decay constant Γ) convolved with the temporal profile of the pulse.

B. Experimental challenges

The experimental measurement of the scattered-light spectra and second-order correlations calculated above for the case when the excitation source is a frequency comb poses significant practical challenges. In general, stabilization of the frequency comb may be required in order to not blur out the

spectral features over the measurement duration. However, even without active laser cavity stabilization, commonly used commercial Ti:sapphire mode-locked lasers can produce pulses with comb linewidths smaller than their pulse repetition rate as long as the integration time is short enough compared to the time scale of environmental perturbations (typically ∼1s). Scanning Fabry-Perot spectral measurements are typically performed using sweeps on the ms time scale. Therefore, in the measured scattered-light spectrum, the separation between individual comb peaks (the laser repetition rate $\delta/2\pi$) should be resolvable.

Perhaps one reason that the scattered-light spectrum from a two-level system under pulsed excitation has not been reported before is due to the stringent requirements imposed on the measurement instrument. To resolve the relevant features, the latter must be able to sample a spectrum with very high resolution over a relatively large range of frequencies. For instance, a scanning Fabry-Perot interferometer able to produce the simulated data above would require a resolution of about 20 MHz, but at the same time a free spectral range of order 100 GHz. That in turn implies a cavity finesse of 5000 with low loss, and frequency stabilization over the period of a measurement (typically ∼1 s). Such instruments are not readily available commercially.

Finally, in practice the frequency-comb spectral bandwidth cannot be excessively large, otherwise contributions from other QDs with different resonance frequencies in close proximity to the QD under test will mask the measured spectrum. In particular, contributions from off-resonant coherent scattering may be most problematic.

XI. CONCLUSIONS

In conclusion, a comprehensive theoretical description of resonant light scattering of a laser frequency comb by a two-level system has been given. Unlike previous approaches describing single-pulse or monochromatic scattered-light spectra, we are able to rigorously account for realistic experimental features which result from the time-averaged measurement involving millions of single pulses for both first-order correlations (spectra) and second-order correlations (photon statistics). Using parameters corresponding to typical experimental conditions, e.g., excitation by a mode-locked Ti:sapphire oscillator with pulse repetition frequency of order 100 MHz and values for commonly grown InAs QDs, we find that coherent light scattering plays a significant role even at high Rabi frequencies. Furthermore, we also see that complete pulse-integrated photon antibunching can only be expected for input pulse areas of less than π. Spectral diffusion was included and shown to capture subtle differences, in particular for the spectra of coherently scattered light. By comparison with experimental data for bichromatic excitation, we have verified in detail these effects. Under certain conditions, the degree of photon antibunching can be rather elevated. These conditions include one in which the scattering is dominated by coherent scattering, thus implying that the generated single-photon wave packet maintains a fixed phase relationship with the incoming laser. The formalism described here can also be extended in a straightforward manner to include resonances with a three-dimensionally-confining optical microcavity, which may be of interest for a variety of applications in quantum-information science.

ACKNOWLEDGMENTS

The authors acknowledge the use of the services provided by Research Computing at the University of South Florida, as well as financial support from the National Science Foundation (NSF Grant No. 1254324).

[1] B. R. Mollow, Phy. Rev. **188**, 1969 (1969).
[2] T. D. Ladd, F. Jelezko, R. Laflamme, Y. Nakamura, C. Monroe, and J. L. O'Brien, Nature **464**, 45 (2010).
[3] J. Beugnon, M. P. A. Jones, J. Dingjan, B. Darquié, G. Messin, A. Browaeys, and P. Grangier, Nature **440**, 779 (2006).
[4] J. Hofmann, M. Krug, N. Ortegel, L. Gérard, M. Weber, W. Rosenfeld, and H. Weinfurter, Science **337**, 72 (2012).
[5] P. Maunz, D. L. Moehring, S. Olmschenk, K. C. Younge, D. N. Matsukevich, and C. Monroe, Nat. Phys. **3**, 538 (2007).
[6] R. Lettow, Y. L. A. Rezus, A. Renn, G. Zumofen, E. Ikonen, S. Götzinger, and V. Sandoghdar, Phys. Rev. Lett. **104**, 123605 (2010).
[7] S.V. Polyakov, A. Muller, E. B. Flagg, A. Ling, N. Borjemscaia, E. Van Keuren, A. Migdall, and G. S. Solomon, Phys. Rev. Lett. **107**, 157402 (2011).
[8] H. Bernien, L. Childress, L. Robledo, M. Markham, D. Twitchen, and R. Hanson, Phys. Rev. Lett. **108**, 043604 (2012).
[9] A. Muller, E. B. Flagg, P. Bianucci, X. Y. Wang, D. G. Deppe, W. Ma, J. Zhang, G. J. Salamo, M. Xiao, and C. K. Shih, Phys. Rev. Lett. **99**, 187402 (2007).
[10] E. B. Flagg, A. Muller, J. W. Robertson, S. Founta, D. G. Deppe, M. Xiao, W. Ma, G. J. Salamo, and C. K. Shih, Nat. Phys. **5**, 203 (2009).
[11] N. Vamivakas, Y. Zhao, C.-Y. Lu, and M. Atatüre, Nat. Phys. **5**, 198 (2009).
[12] S. Ates, S. M. Ulrich, S. Reitzenstein, A. Löffler, A. Forchel, and P. Michler, Phys. Rev. Lett. **103**, 167402 (2009).
[13] S. Ates, I. Agha, A. Gulinatti, I. Rech, M. T. Rakher, A. Badolato, and K. Srinivasan, Phys. Rev. Lett. **109**, 147405 (2012).
[14] A. Ulhaq, S. Weiler, S. M. Ulrich, R. Roßbach, M. Jetter, and P. Michler, Nat. Photon. **6**, 238 (2012).
[15] H. S. Nguyen, G. Sallen, C. Voisin, Ph. Roussignol, C. Diederichs, and G. Cassabois, Appl. Phys. Lett. **99**, 261904 (2011).
[16] C. Matthiesen, A. N. Vamivakas, and M. Atatüre, Phys. Rev. Lett. **108**, 093602 (2012).
[17] K. Konthasinghe, J. Walker, M. Peiris, C. K. Shih, Y. Yu, M. F. Li, J. F. He, L. J. Wang, H. Q. Ni, Z. C. Niu, and A. Muller, Phys. Rev. B **85**, 235315 (2012).
[18] M. Metcalfe, S. M. Carr, A. Muller, G. S. Solomon, and J. Lawall, Phys. Rev. Lett. **105**, 037401 (2010).

[19] C. Matthiesen, M. Geller, C. H. H. Schulte, C. Le Gall, J. Hansom, Z. Li, M. Hugues, E. Clarke, and Mete Atatüre, Nat. Commun. **4**, 1600 (2013).
[20] H. S. Nguyen, G. Sallen, C. Voisin, Ph. Roussignol, C. Diederichs, and G. Cassabois, Phys. Rev. Lett. **108**, 057401 (2012).
[21] K. Konthasinghe, M. Peiris, Y. Yu, M. F. Li, J. F. He, L. J. Wang, H. Q. Ni, Z. C. Niu, C. K. Shih, and A. Muller, Phys. Rev. Lett. **109**, 267402 (2012).
[22] D. P. S. McCutcheon and A. Nazir, Phys. Rev. Lett. **110**, 217401 (2013).
[23] A. Ulhaq, S. Weiler, C. Roy, S. M. Ulrich, M. Jetter, S. Hughes, and P. Michler, Opt. Express **21**, 4382 (2013).
[24] Y. Zhu, Q. Wu, A. Lezama, D. J. Gauthier, and T. W. Mossberg, Phys. Rev. A **41**, 6574 (1990).
[25] M. A. Newbold and G. J. Salamo, Phys. Rev. A **22**, 2098 (1980).
[26] G. S. Agarwal, Y. Zhu, D. J. Gauthier, and T. W. Mossberg, J. Opt. Soc. Am. B **8**, 1163 (1991).
[27] Z. Ficek and H. S. Freedhoff, Phys. Rev. A **48**, 3092 (1993).
[28] D. L. Aronstein, R. S. Bennink, R. W. Boyd, and C. R. Stroud Jr., Phys. Rev. A **65**, 067401 (2002).
[29] M. Peiris, K. Konthasinghe, Y. Yu, Z. C. Niu, and A. Muller, Phys. Rev. B **89**, 155305 (2014).
[30] K. Rzążewski and M. Florjanczyk, J. Phys. B **17**, L509 (1984).
[31] M. Florjanczyk, K. Rzążewski, and J. Zakrzewski, Phys. Rev. A **31**, 1558 (1985).
[32] M. Lewenstein, J. Zakrzewski, and K. Rzążewski, J. Opt. Soc. Am. B **3**, 22 (1986).
[33] L. F. Roberto Buffa, Stefano Cavalieri, and M. Matera, J. Phys. B **21**, 239 (1988).
[34] P. Rodgers and S. Swain, Opt. Commun. **81**, 291 (1991).
[35] A. Moelbjerg, P. Kaer, M. Lorke, and J. Mørk, Phys. Rev. Lett. **108**, 017401 (2012).
[36] W. Zhang and W. Tan, J. Opt. Soc. Am. B **4**, 1885 (1987).
[37] R. J. Temkin, J. Opt. Soc. Am. B **10**, 830 (1993).
[38] Z. Ficek, J. Seke, A. V. Soldatov, and G. Adam, Phys. Rev. A **64**, 013813 (2001).
[39] A. Muller, Q. Q. Wang, P. Bianucci, C. K. Shih, and Q. K. Xue, Appl. Phys. Lett. **84**, 981 (2004).
[40] C. Santori, D. Fattal, J. Vuckovic, G. S. Solomon, E. Waks, and Y. Yamamoto, Phys. Rev. B **69**, 205324 (2004).
[41] P. Borri, W. Langbein, S. Schneider, U. Woggon, R. L. Sellin, D. Ouyang, and D. Bimberg, Phys. Rev. Lett. **87**, 157401 (2001).